

Fiber method analysis of rc beam retrofitted with turnbuckle external post-tensioning

Bernardo A. Lejano*

Department of Civil Engineering, De La Salle University, 2401 Taft Avenue, Manila, Philippines

(Received May 24, 2015, Revised December 6, 2015, Accepted December 24, 2015)

Abstract. Strengthening as well as correcting unsightly deflections of reinforced concrete (RC) beam may be accomplished by retrofitting. An innovative way to do this retrofitting that is proposed in this study utilizes turnbuckle to apply external post-tensioning. This Turnbuckle External Post-Tensioning (T-EPT) was experimentally proven to improve the serviceability and load carrying capacity of reinforced concrete beams. The T-EPT system comprises a braced steel frame and a turnbuckle mechanism to provide the prestressing force. To further develop the T-EPT, this research aims to develop a numerical scheme to analyze the structural performance of reinforced concrete beams with this kind of retrofitting. The fiber method analysis was used as the numerical scheme. The fiber method is a simplified finite element method that is used in this study to predict the elastic and inelastic behavior of a reinforced concrete beam. With this, parametric study was conducted so that the effective setup of doing the T-EPT retrofitting may be determined. Different T-EPT configurations were investigated and their effectiveness evaluated. Overall, the T-EPT was effective in improving the serviceability condition and load carrying capacity of reinforced concrete beam.

Keywords: fiber method, retrofitting, external post-tensioning, reinforced concrete beam, turnbuckle

1. Introduction

Nowadays, civil engineers are faced with problems of aging structures specially reinforced concrete (RC). Inevitable long term environmental exposure and over loading usually affect the structural performance of RC members. Deterioration of materials, increase in service loads, and other environmental factors caused some structural members, usually the beams, to exhibit unsightly deflections and cast doubt in their strength. According to Suprenant and Malisch (2009), by incorporating post-tensioning, the deflection and tolerances of the structural member is controlled and minimized. Aptly, external post-tensioning is an ideal retrofitting technique wherein external tendons are used to apply axial compressive force and bending moment in order to improve serviceability and load carrying capacity of a structural member. Klaiber *et al.* (1981) reported that post-tensioning solved the problem of deformation of steel bridges by reducing the tensile strain in the bottom flanges. Daly and Witarnawan (1997) studied two externally post-

*Corresponding author, Dr. Eng'g., E-mail: bernardo.lejano@dlsu.edu.ph

tensioned bridges and concluded that the strengthening of both bridges greatly relied on the strength of the cables followed by the strength of the anchorage. Nordin (2004) provided a good literature review on strengthening of structures with externally prestressed tendons, classified into steel and fiber-reinforced polymer (FRP) tendons. Some of the recent experimental research works using steel tendons were reported by Naghipour *et al.* (2010), Shin and Lee (2010), Shin *et al.* (2014), Lee *et al.* (2015). FRP materials can be a good substitute to steel for external tendons because they are not affected by environmental influences in the same way as steel. Recent experimental researches that have used carbon FRP (CFRP) tendons include Elrefai *et al.* (2012), Matta *et al.* (2009), Bennitz *et al.* (2012). Furthermore, considerable improvement in shear resistance is achieved by external post-tensioning as reported by El-Shafiey and Atta (2012). Moreover, Lee *et al.* (2010) developed a computational method that predicts the shear strengthening effect of RC beams with externally unbonded high-tensioned steel rods.

External post-tensioning is usually accomplished using hydraulic jacks. One of the objectives of this study is to find cheaper and simpler alternative. One way is by doing away with hydraulic jacks. According to Shin *et al.* (2014), steel rods can be post-tensioned simply by tightening nuts or turnbuckles at the rod end. Likewise, previous studies of the author with Adiaz *et al.* (2011), and Astillero *et al.* (2013) showed that a simple turnbuckle may be used to apply the prestressing force in retrofitting steel beams. The current research is being conducted to study the applicability of external post-tensioning using turnbuckle for RC beams. However, the behavior of RC is more complex than steel. The stress-strain curve of concrete is nonlinear as compared to steel which can be represented by bilinear model. In addition, the concrete behaves differently in tension and compression, and its behavior is made more complicated by crack propagation. Lastly, the calculation becomes very difficult because external tendons are usually unbonded hence the strain compatibility between concrete and tendon cannot be used.

Recent works on providing computational approach to analyze RC beams with unbonded tendons have been done by Shin *et al.* (2014), Kim and Lee (2012), Tan and Kong (2009), Au *et al.* (2009), Du *et al.* (2008). Shin *et al.* (2014) proposed a formula for moment capacity but for RC beam with a V-shaped EPT rod system that they developed. Numerical model for unbonded prestressed concrete were also developed by Kim and Lee (2012), Au *et al.* (2009), Du *et al.* (2008) to predict the behavior before and after cracking, under service load, and ultimate condition. Their model gave good agreement with experiment results. Also, they were able to identify parameters that influenced the behavior of unbonded prestressed beams. While Tan and Kong (2009) established design equations for direct determination of external tendon area and eccentricity to strengthen a simple-span, reinforced concrete beam.

To be able to do the calculations parallel to the experimental tests conducted, a fiber method model was developed in this study. The fiber method is expected to be able to simulate the behavior of RC beams up to the ultimate stage, including possible loading, unloading, and reloading stages. The fiber method is also known as “fiber beam method” or “fiber beam model” or simply “fiber model”. Using the fiber method, parametric study was conducted to identify the factors that can make the external post-tensioning using turnbuckle more effective and economical.

2. Experimental program

The author, together with Adiaz and Vidad (2011), first conducted experimental study on the use of turnbuckle in external post-tensioning of steel wide flange beam to retrofit it. Constant

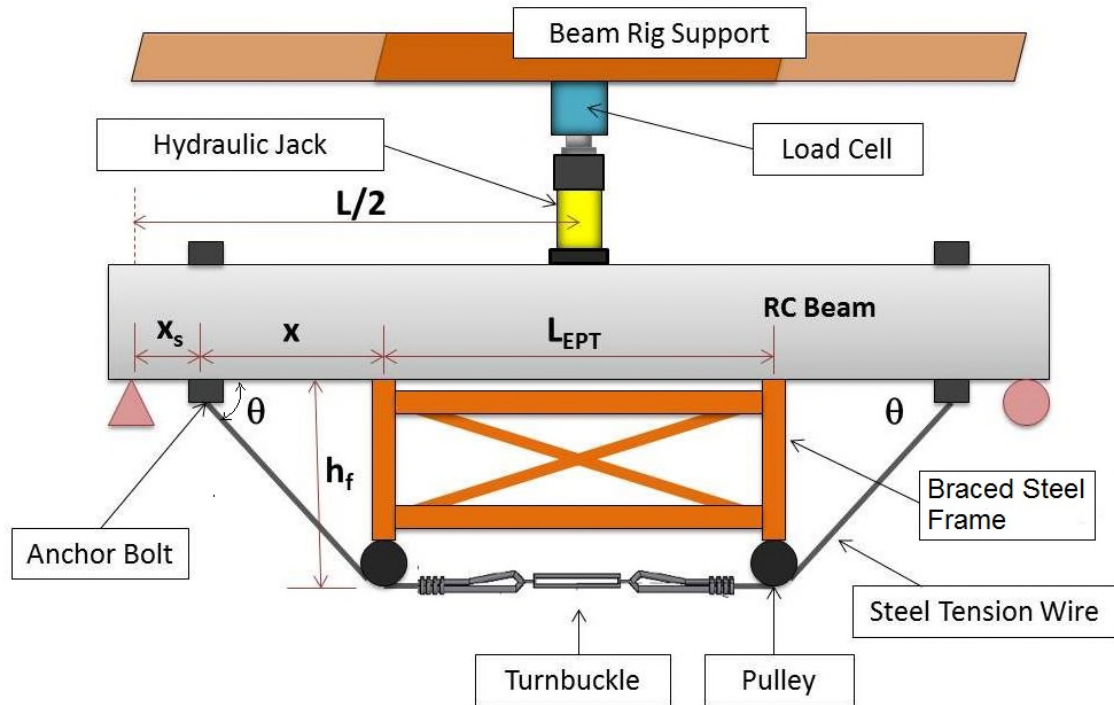


Fig. 1 Experimental test setup of RC beam retrofitted with T-EPT

eccentricity was achieved by connecting the tendons to vertical posts serving as anchorages near the ends of the beam. The results were very promising, but showed weakness in the form of weld fracture at the anchorage-beam connection. To avoid this problem at the anchorage, harped configuration of the tendon was adopted in the subsequent research of Astillero *et al.* (2013). The harped tendon configuration was achieved by placing deviators at two points in the beam. Indeed, this yielded more effective results, but exhibited some instability in the deviator. Almost similar configuration using deviators placed at two points were adopted by Bennitz *et al.* (2012) and Elrefai *et al.* (2008) but used hydraulic jack. On the other hand, Matta *et al.* (2009) also used turnbuckle but adopted CFRP tendon with single deviator at the midspan. Shin *et al.* (2014) used V-shaped post-tensioning steel rod system. They applied post-tensioning by tightening the nuts at the special anchorages at the ends of the steel rods. They extended their study (Lee *et al.* 2015) to continuous beams and used also turnbuckle in prestressing.

In this study, harped tendon configuration is adopted but using braced steel frame as the deviator. Drawing of the external post-tensioning retrofit setup used in the experiment is shown in Fig. 1. Hereafter, this retrofit will be referred to as Turnbuckle External Post-tensioning or “T-EPT”. The external moment is produced by applying a concentrated load at midspan. The T-EPT system used in the experiment may look quite big compared to the beam specimen because the beam is scaled down to fit into the testing rig. However, in actual application it will be supporting larger beams. Furthermore, the size of the steel frame is dependent on the size of the turnbuckle available.

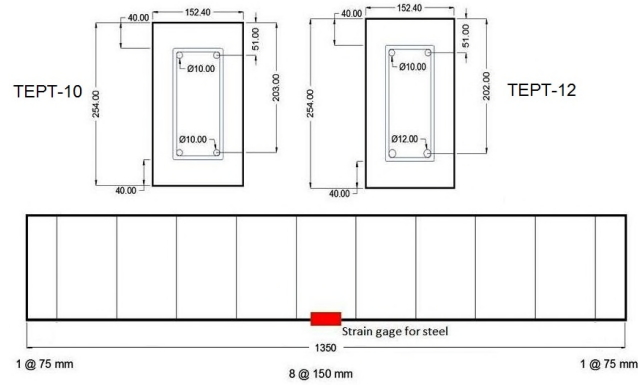


Fig. 2 Details of RC beam specimen

2.1 Beam specimens

Results from four RC beam specimens were used in this study. These are part of the specimens tested by the author with Peñamante *et al.* (2015). The concrete used has a compressive strength of 21 MPa and deformed reinforcing steel bar has a yield strength of 300 MPa. The beam specimens have to be scaled down due to the size limitations of the beam testing rig. Shown in Fig. 2 are the dimensions of the beam. The beam has a total length of 1.35 m and a clear span length (L) of 1.2 m. The figure also shows two cross-sections of the beam. The first shows reinforcement of 10 mm diameter bars both for top and bottom bars while the second differed as it has 12 mm diameter bars for the bottom bars. Both cases can be easily verified as under-reinforced, ensuring that the tension steel will yield. The specimens were divided into these two reinforcing details (TEPT-10 and TEPT-12 representing the two reinforcing details, respectively). To verify the yielding of steel, strain gages were attached to the bottom bars at midspan as shown in the figure. Displacement transducers were also used to monitor the midspan deflection.

2.2 Loading procedure

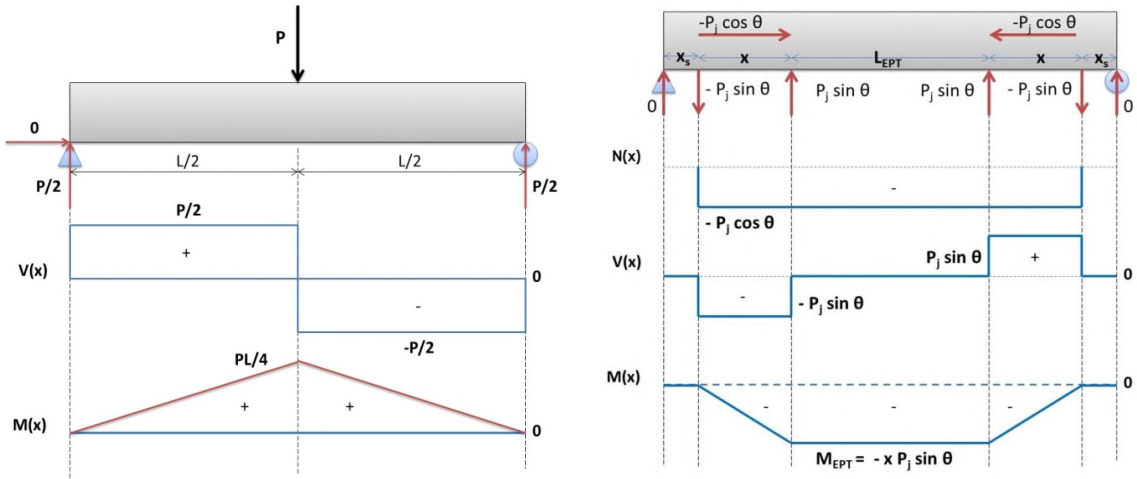


(a) Beam without T-EPT



(b) Beam with T-EPT

Fig. 3 Actual test set-up



(a) Shear and moment diagram due to external load (b) Axial, shear and moment diagram due to T-EPT

Fig. 4 Effects of forces on the beam

The RC beam specimens were loaded with concentrated force at midspan. The loading applications were done for elastic, inelastic, and ultimate conditions. The loading sequences were as follows: (1) first - loading to a specified midspan deflection, i.e., deflection at first yielding of the bottom bars (2) second - unloading, (3) third - application of the T-EPT to recover from residual deflection, and (4) fourth - reloading with the T-EPT applied.

The concentrated load is first applied so as to produce the initial midspan deflection. In the experiment, this initial displacement is set corresponding to the first yielding of the beam. Fig. 3 shows the actual beam rig test set-up. The shear and moment diagram resulting from this external load is shown in Fig. 4(a). The maximum bending moment is at the midspan. The positive bending moment will cause the downward deflection of the beam.

2.3 The T-EPT system

As shown in Fig. 1, the T-EPT system is composed of the braced steel frame and 15.9 mm in diameter Grade 250 ($f_{py}=1465$ MPa, $f_{pu}=1720$ MPa) stranded wire steel tendon with turnbuckle attached at the middle. The materials were selected making sure that they are readily available in local hardware shops. As the turnbuckle is turned, it provides the prestressing force. The steel frame is made of angle bars, which is so designed to transmit the jacking force to the beam. Pulleys were attached to the frame where the stranded wire tendon would pass to ensure that no friction will develop between the tendon and the steel frame. The frame has a height of hf and a length of L_{EPT} . The inclined tendon makes an angle of θ with respect to the member-axis of the beam. With this configuration, the T-EPT system will be able to transmit forces to the beam as shown in Fig. 4(b). Also shown in the figure are the resulting axial, shear and bending moment diagrams. With these forces applied, negative bending moment is produced causing the beam to deflect upwards. This is the basic concept how the beam is restored to its undeflected condition.

3. Formulation of numerical model

The T-EPT follows the same principle as prestressing wherein axial force and moment are applied to the beam with the use of tension cables to counteract the deflection and moments induced by the external load(s) on the beam. When the T-EPT is acting, the moment equilibrium condition of the beam may be written as shown in Eq. (1).

$$M_{EXT} = M_{Beam} + M_{EPT} \quad (1)$$

The external moment, M_{EXT} , can be easily determined if the external force is given as shown in the moment diagram in Fig. 4(a). Also, the moment due to the T-EPT, M_{EPT} , can be determined if the jacking force is known as shown in Fig. 4(b). However, the jacking force (which will be termed as P_j) depends on the deflection of the beam that needed to be counteracted. Vice-versa, the resistance of the beam is also affected by the jacking force. Hence, it is salient that the moment resisted by the RC beam, M_{Beam} , be determined accurately. One way to do this is by means of finite element method. Lou and Xiang (2006) performed a numerical model based on the finite element method for the nonlinear analysis of concrete beams prestressed with external tendons. The effects of external tendons were expressed as equivalent nodal loads acting on the beam. Results predicted by the finite element analysis were in good agreement with the experimental data. Afterwards, Lou *et al.* (2013) also used the finite element method for the full-range analysis of continuous externally prestressed concrete beams. In this study, simpler model in the form of fiber method and limited to simply supported beam was tried.

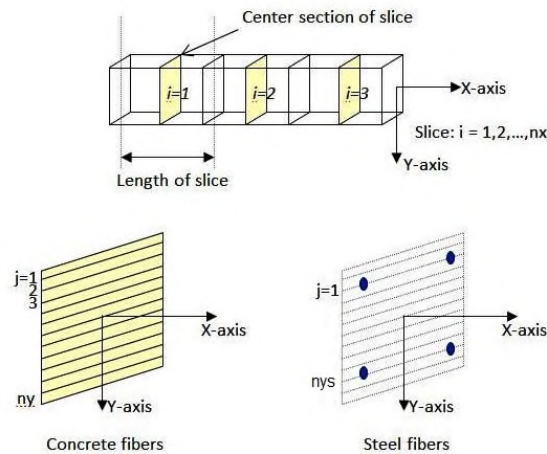


Fig. 5 Typical fiber method modeling of RC beam

3.1 Numerical modeling using fiber method

The fiber method can be defined as a simplified one-dimensional finite element method analysis. Probably, Mark and Rosset (1971) were the first to investigate the applicability of the fiber method. Kaba and Mahin (1984) used a flexibility approach in formulating the fiber method

used in modeling reinforced concrete for seismic analysis. Lejano (1995), with Shirai *et al.* (1996), used fiber method in studying the flexural behavior of high strength RC columns subjected to high and fluctuating axial load. Spacone *et al.* (1996) also implemented the fiber discretization of the section behavior with axial force and bending moment interaction. Lejano (2007) extended the use of fiber method in the investigation of biaxial bending of RC columns. Mullapudi and Ayoub (2013) even formulated a more sophisticated fiber model based on the Timoshenko beam theory, with a fiber section being able to account for combined axial, flexure, shear and torsional effects. However, in this study only bending moment and axial force were considered. Moreover, it is assumed that the governing failure mode is flexure. Shear failure, anchorage failures, and other failures are not considered in this study.

In fiber method, the discretized element is treated as a fiber with resistance effective only in the direction of its length. The fiber method is accomplished by dividing the beam into slices along the member axis (x -axis), and the slices are further subdivided into concrete fibers and steel fibers (along y -axis). A typical subdivision of the beam by fiber method is shown below in Fig. 5. As a general rule, the length of slice at the critical section is one-half of the member depth. This is based on the work of Kitajima (1994). This is to prevent unrealistic localized damage if very fine slice is used and deviation from experiment results if very coarse slice subdivision is adopted.

By considering the uniaxial stress-strain relationship of each fiber, the average forces of a section can be calculated by summing up the resisting forces of all fibers in that particular section i . This is shown in Eq. (2).

$$\Delta N_i = \sum (A_{ij})(\Delta \sigma_{ij}) \quad \Delta M_i = \sum (A_{ij})(\Delta \sigma_{ij})(Y_j) \quad (2)$$

where N_i = axial force at section i , M_i = moment at section i , A_{ij} = cross-sectional area of the fiber, σ_{ij} = fiber stress, Y_j = distance of the centroid of fiber "j" from the centroid of the section, i = index counter of section along x -axis, j = index counter of fiber along y -axis. By substituting the elastic stress-strain relationship and expressing the section deformation vector in terms of the centroidal axial strain (ε_{oi}) and section curvature (ϕ_i), the stiffness matrix of the section can be established.

$$\begin{Bmatrix} \Delta N_i \\ \Delta M_i \end{Bmatrix} = \begin{bmatrix} k_{i11} & k_{i12} \\ k_{i21} & k_{i22} \end{bmatrix} \begin{Bmatrix} \Delta \varepsilon_{oi} \\ \Delta \phi_i \end{Bmatrix} \quad (3)$$

To implement the fiber method, taking into account the non-linearity of the behavior of materials, the incremental analysis procedure making use of the initial stiffness method is adopted. This is an iteration process within each incremental load step wherein the unbalanced force vector is successively calculated until it becomes very small to say that the numerical solution has converged. The unbalance force is the difference between the force calculated based on the initial stiffness (Eq.(3)) and the actual force calculated from the stresses that developed in the materials. For example, $\Delta M_i'' = \Delta M_i' - \Delta M_i$, where $\Delta M_i''$ is the unbalance moment, ΔM_i is the actual moment calculated based on the fiber stresses, and $\Delta M_i'$ is the moment calculated from the initial stiffness of section i . For the slices, the governing matrix equation is shown below in Eq. (4).

$$\begin{Bmatrix} \Delta N_i \\ \Delta M_i \end{Bmatrix} + \begin{Bmatrix} \Delta N_i'' \\ \Delta M_i'' \end{Bmatrix} = \begin{bmatrix} k_{i11} & k_{i12} \\ k_{i21} & k_{i22} \end{bmatrix} \begin{Bmatrix} \Delta \varepsilon_{oi} \\ \Delta \phi_i \end{Bmatrix} \quad (4)$$

On member level, the member force vector, $\{\Delta P\}$, is related to the section force vector, $\{\Delta P_i\}$, through the connectivity matrix $[B_i]$, that is $\{\Delta P_i\} = [B_i]\{\Delta P\}$. This matrix $[B_i]$ can easily be

established by following the axial force distribution along the length of the beam and moment diagram as shown in Fig. 4(a). Following the concept of virtual work method, almost the same equation as in Eq. (4) is obtained as shown in Eq. (5). In this study, only half of the beam is modeled such that ΔN and ΔM are the increment axial force and bending moment at the midspan. The unknown vector to be computed is $\{\Delta\delta\}$.

$$\{\Delta P\} + \{\Delta P''\} = [K]\{\Delta\delta\} \quad (5)$$

where $[K]$ =member stiffness matrix, $\{\Delta P\}$ =member force vector= $[\Delta N, \Delta M]^T$, $\{\Delta P''\}$ =unbalanced member force vector= $[\Delta N'', \Delta M'']^T$, $\{\Delta\delta\}$ =member displacement vector= $[\Delta\delta_a, \Delta\delta_f]^T$, $\Delta\delta_a$ =axial displacement at midspan, and $\Delta\delta_f$ =flexural displacement at midspan. The member stiffness matrix and unbalanced force vector may be calculated as follows

$$[K] = \sum_{i=1}^{nx} \int_{x1}^{x2} [Bi]^T [ki]^{-1} [Bi] dx \quad [\Delta P''] = \sum_{i=1}^{nx} \int_{x1}^{x2} [Bi]^T [ki]^{-1} \{\Delta P_i''\} dx \quad (6)$$

The computer implementation (using Visual Basic) of the fiber method is done by applying the loads at increment. The simulation is done by first applying a concentrated load at the midspan until the beam yields, that is, the bottom bar yields. Then unloading is done by incrementally removing the concentrated load. Due to the nonlinearity of the material residual deflection will develop. Then, the beam is applied with the T-EPT to counteract the residual deformation. The axial force and moment due to T-EPT were incrementally applied at the central section of each slice following the distribution of forces shown in Fig. 4(b). After that, the beam is loaded again with the concentrated load at midspan. At this stage, the incremental strain in the tendon is assumed to be equal to the incremental axial displacement of the member divided by the total length of the tendon.

3.2 Constitutive model of materials

It can be easily seen that the accuracy of the fiber method is critically dependent on the constitutive law of concrete and steel. In this study, the exponential stress-strain curve developed by Lejano (2009) was used as a constitutive model for concrete. The equation for the ascending

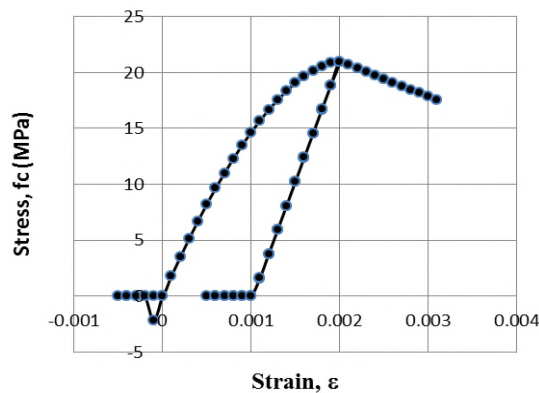


Fig. 6 Sample output of exponential stress-strain relationship of concrete

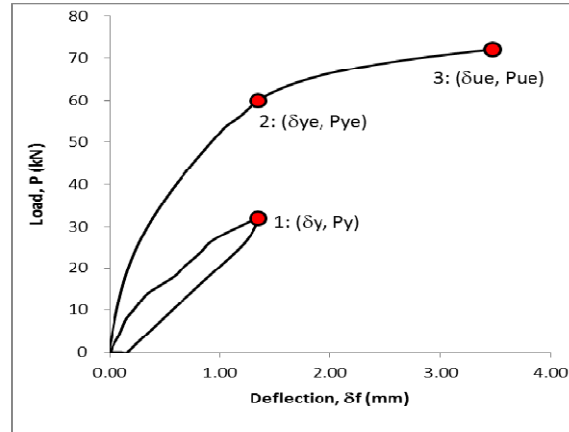


Fig. 8 Typical load-displacement curve showing critical points (1) yielding-without T-EPT, (2) yielding - with T-EPT and (3) ultimate - with T-EPT

branch of the stress-strain curve of this model is shown in Eq. (7). The descending branch is linear from peak stress up to the ultimate strain of 0.003. The unloading branch follows a linear relationship with a slope E_c . A sample stress-strain curve depicting loading, unloading, and reloading is shown in Fig. 6.

$$f_c = f_c' \left[1 - \left(\frac{\varepsilon_p - \varepsilon}{\varepsilon_p} \right)^b \right] \quad (7)$$

where f_c = stress of concrete for the corresponding strain (ε), f_c' = compressive strength of concrete, ε_p = strain at peak stress = $0.018 + 0.00001 f_c'$, and $b = 2 - 0.0125 f_c'$. For the steel bars, the model first developed by Ciampi *et al.* (1982) was used. The Ciampi model has been used by many researchers and has been tested extensively to give a realistic and accurate stress-strain relationship of steel.

4. Results

In this section the results of numerical investigation of the behavior of RC beam retrofitted with T-EPT using fiber method are presented. The parameters that were investigated are the load and deflection at yield (P_{ye} and δ_{ye}) and load and deflection at ultimate (P_{ue} and δ_{ue}) when the T-EPT is acting. These parameters were compared to the load and deflection at yield of the beam when the T-EPT is not yet acting. Shown in Fig. 8 is a typical load-displacement curve of the beam. Indicated in the figure are the critical points that were observed: (1) Yielding - Without T-EPT, (2) Yielding - With T-EPT, and (3) Ultimate - With T-EPT

4.1 Verification of numerical results

The loading of the beam specimens were simulated by fiber method with the following dimensions taken into account: $X_s = 70$ mm, $X = 300$ mm, $L_{EPT} = 460$ mm, $h_f = 350$ mm (refer to

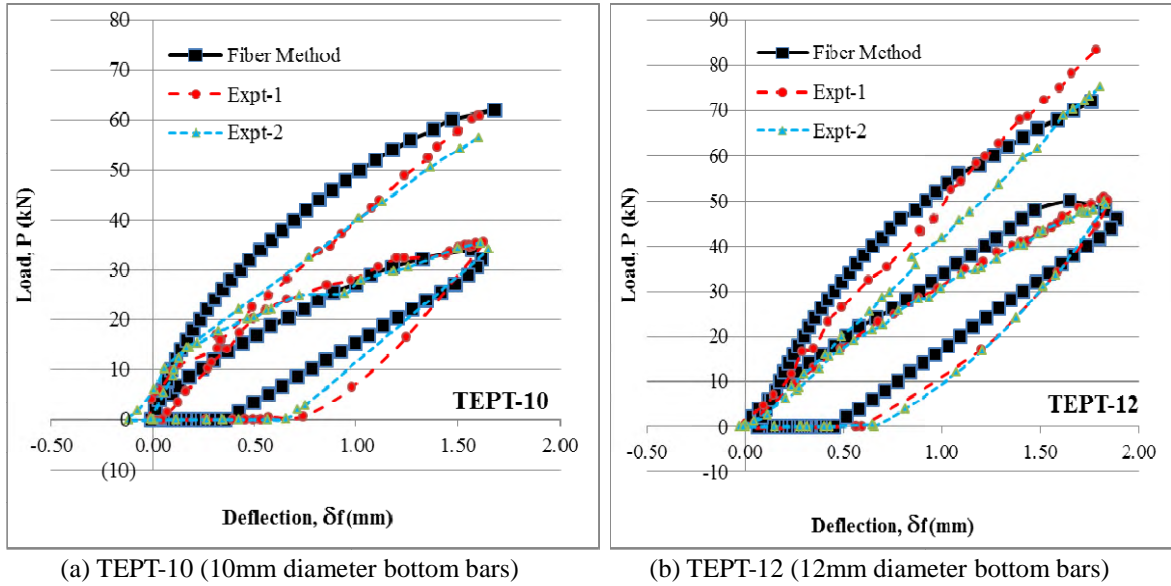


Fig. 7 Comparison of $P-\delta_f$ curve between fiber method & experiment results

Fig. 1). The concentrated load was applied gradually at an interval of 1 kN, until the bottom bar yields. Then the load is gradually decreased until no load is applied. After this, the residual deflection at the midspan is counteracted by applying the T-EPT, which is equivalent to the force shown in Fig. 4(b). The jacking force, P_j , is gradually increased until the deflection at midspan is eliminated. Then the concentrated load is gradually reapplied at 1 kN interval until a deflection causing yielding of the bottom bars is obtained. The results of the fiber method are shown in Fig. 7. It is plotted with the experiment results obtained from the work of the author, together with Peñamante *et al.* (2015). It can be seen that there is substantially good agreement between the fiber method results and the experiment results. Although, there are differences, the values at critical points agreed very well. The differences observed are: (1) Difference in the slope during unloading. (2) The actual reloading is almost linear while the fiber method gives a more curved reloading path. These may be attributed to other factors not considered in the fiber method like the additional degradation of concrete during unloading/reloading and possible movement at the support. The same observation was mentioned in a parallel study of Toral and Lejano (2015).

To verify the accuracy of the fiber method results, the load and displacement at yield (P_y and δ_y) are compared with experiment results and conventional calculation results. The conventional calculation of P_y is done by calculating the moment resisted by the section when the bottom bars are yielding and the stress block in the compression zone is assumed linear with $0.70f_c'$ as the stress in the outermost compression fiber (Park and Pauley 1975). The deflection at yielding is calculated using the elastic formula for the deflection shown in Eq. (8), with the correction factor applied to the moment of inertia due to the cracking of concrete as stipulated in Eqs. (10)-(9) of section 10.10.4.1 of ACI-318 (2008).

$$\delta = \frac{PL^3}{48EI(cf)} \quad \text{where } cf = \text{correction factor} = (0.1 + 25\rho)(1.2 - 0.2b_w/d) \quad (8)$$

Table 1 Comparison of experiment, fiber method, and conventional calculation

Specimen		Expt (Ave.)	FM	Calc	FM/Expt	FM/Calc
TEPT-10 (Load)	Py (kN)	34.5	30	29.8	0.96	1.11
	Pye (kN)	58.6	62	-	1.06	-
	Pue (kN)	67.8	73	-	1.08	-
TEPT-10 (Deflection)	δy (mm)	1.620	1.176	1.006	0.73	1.18
	δye (kN)	1.603	1.379	-	0.86	-
	δue (kN)	3.918	3.446	-	0.88	-
TEPT-12 (Load)	Py (kN)	50.1	45	41.3	0.96	1.08
	Pye (kN)	79.3	74	-	0.93	-
	Pue (kN)	84.7	87	-	1.03	-
TEPT-12 (Deflection)	δy (mm)	1.828	1.291	1.116	0.76	1.15
	δye (kN)	1.793	1.372	-	0.77	-
	δue (kN)	4.381	3.266	-	0.75	-

The comparison is tabulated in Table 1 for beam specimens TEPT-10 and TEPT-12. It may be said that the fiber method results are in satisfactory agreement with the experiment and conventional calculation results. Better agreement is observed in the loads than in the deflections. The experiment gave larger deflections indicating that probably there are other sources of the measured deflection, such as movement in the roller support and/or additional degradation of concrete. At yield condition, it can be seen that the values obtained from fiber method are in between the experiment results and the conventional calculation results. However, in terms of the load, the fiber method gave conservative results as compared to the experiment results. Moreover, the conventional calculation gave more conservative values. Hence, the fiber method and the conventional calculation would result to a safer condition if adopted in design work.

However, when the T-EPT is acting, such as in (Pye, δye) and (Pue, δue), the conventional calculation cannot be done because the strain compatibility between the tendon and concrete cannot be applied since the tendon is unbonded. These difficulties have also been recognized in the works of Lee *et al.* (2011) and Au *et al.* (2009). Furthermore, the concrete and steel reinforcements have undergone strains during the loading and unloading, such that when T-EPT is applied, the

Table 2 Comparison of fiber method with conventional calculation for different bar diameter

	Bar Diameter	FM	Calc	FM/Calc
Load at Yield Py (kN)	8 mm	22	19.9	1.11
	10 mm	30	29.8	1.01
	12 mm	42	41.2	1.02
	16 mm	76	68.4	1.11
Deflection at Yield δy (mm)	8 mm	1.101	0.84	1.31
	10 mm	1.176	1.006	1.17
	12 mm	1.297	1.115	1.16
	16 mm	1.595	1.231	1.30

Table 3 Tabulation of the effect of length of steel frame (L_{EPT})

L_{EPT} (mm)	60	160	260	360	460	560	660	760	860
L_{EPT}/L	0.050	0.133	0.217	0.300	0.383	0.467	0.550	0.633	0.717
θ (degrees)	35.0	37.9	41.2	45.0	49.4	54.5	60.3	66.8	74.1
P_{ye} (kN)	66.0	66.0	64.0	62.0	62.0	60.0	56.0	52.0	48.0
δ_{ye} (mm)	1.463	1.504	1.438	1.379	1.481	1.478	1.348	1.327	1.315
P_{ye}/P_y	2.20	2.20	2.13	2.07	2.07	2.00	1.87	1.73	1.60
δ_{ye}/δ_y	1.244	1.279	1.223	1.173	1.259	1.257	1.146	1.128	1.118

concrete and steel are already not in their virgin state. Hence, no conventional calculation can be made for (P_{ye} , δ_{ye}) and (P_{ue} , δ_{ue}).

Instead, the results of the fiber method are further verified by again comparing the load and displacement at yield (P_y and δ_y) as affected by the amount of steel reinforcement. To do this, different sizes of bars were used in the fiber method analysis. The top bars and bottom bars are of the same size. The fiber method results are then compared with the conventional calculation. The result of this comparison is shown in Table 2. It can be seen that good agreement were obtained, with the load showing better agreement than the displacement. Take note that the bar sizes were selected to maintain yielding failure mode.

4.2 Effect of braced steel frame dimensions

The effects of the dimensions of the steel frame in the structural performance of the beam and the effectiveness of the T-EPT were investigated by varying the length (L_{EPT}) and the height (h_f) of the steel frame of the beam specimen TEPT-10. The values of the load and displacement at yield obtained from fiber method are $P_y = 30\text{kN}$ and $\delta_y = 1.176\text{ mm}$, respectively.

In the first investigation, the height of the steel frame is fixed at $h_f = 350\text{ mm}$, the actual height of the steel frame used in the experiment. The length of the steel frame used in the experiment was 460 mm. In the numerical simulation, it was varied from a low value of 60 mm and to a high value of 860 mm. Since h_f is constant, the slope (θ) becomes larger as L_{EPT} becomes longer. It was determined that a jacking force of 125 kN is needed to close the residual deflection. This gives a stress of 505 MPa which is about 35% of f_{py} of the stranded wire tendon. Although, Shin *et al.* (2014) recommended a minimum of 40% of f_{py} , the applied jacking force resulted to considerable increase in strength. In all cases, the jacking force was maintained at 125 kN. Shown in Table 3 are the results of the numerical simulations. It can be seen that the value of P_{ye} decreases as the L_{EPT} increases. It follows that the ratio P_{ye}/P_y also decreases as L_{EPT} increases. The trend of P_{ye}/P_y is graphically presented in Fig. 9(a). This means that a shorter steel frame is more effective in increasing the strength of the beam. A shorter frame also means a more economical frame. However, there must be some limit to this because the turnbuckle will not fit into the steel frame if the frame was very short. In Fig. 9(b), the deflection ratio, δ_{ye}/δ_y , is almost constant (although there is slight fluctuation) as L_{EPT} varies. This may mean that the length of the frame does not have much effect on the deflection. In general, it was observed that as the tendon has smaller slope (θ), the T-EPT becomes more effective in increasing the strength of the beam.

Next, the effect of varying the height, h_f , of the steel frame was investigated. Table 4 tabulates

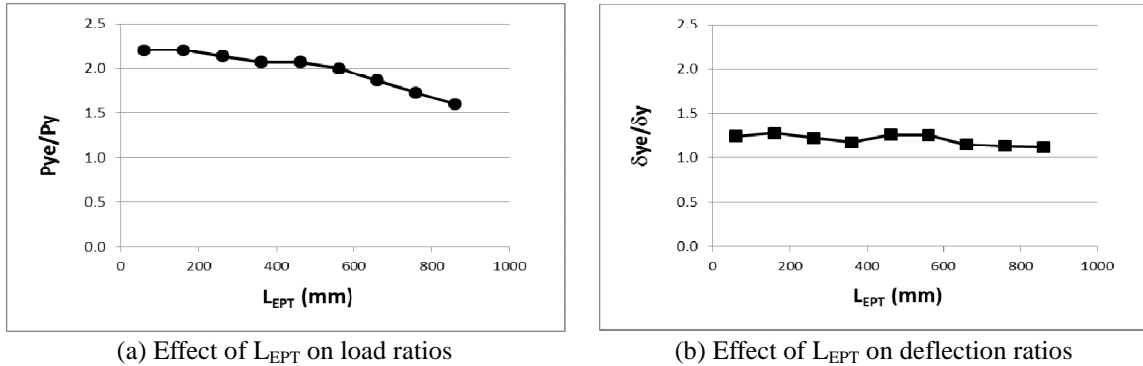


Fig. 9 Plot of the effect of L_{EPT} on load and deflection ratios

the results of the numerical simulations with L_{EPT} fixed at 460 mm, the actual length of the frame used in the experiment. The height, h_f , was varied from 100 to 500 mm. These values were chosen to make the tendon slope smaller. Again, a jacking force of 125 kN was needed to close the residual deflection in all cases. The load P_{ye} and ratio P_{ye}/P_y become smaller as h_f becomes larger. For better visualization, the trend of the load ratio as h_f varies is shown in Fig. 10(a). Based on this, it can be deduced that smaller h_f seems to result to a more effective retrofitting. Shown also are plots when the length is shorter, that is, $L_{EPT} = 160$ mm. It can be seen the P_{ye}/P_y is higher for the shorter L_{EPT} .

In Fig. 10(b), the deflection ratio, δ_{ye}/δ_y , is plotted against h_f . The graph shows that δ_{ye}/δ_y also becomes slightly lower as h_f becomes larger, but with some fluctuations. This seems to indicate that the serviceability may be compromised if the height (h_f) of the frame became very large. Lower values of δ_{ye}/δ_y mean lower serviceability. But, all the values of δ_{ye}/δ_y are greater than one implying improved serviceability. Plots for $L_{EPT} = 460$ mm and $L_{EPT} = 160$ mm are almost identical, indicating that the height h_f has more influence than L_{EPT} on the deflection of the beam.

4.3 Parametric study for actual-sized beams

To investigate the possible application of T-EPT in an actual beam, fiber method simulations were done for larger beam, which will be termed here as “actual-sized” beam. A bigger cross-section is adopted, with width of 200 mm, a total depth of 400mm, and a concrete cover of 50 mm. The length of the beam is 6 m. For this beam, the load and displacement at yield were calculated using fiber method and compared with conventional calculation for different amount of reinforcement. The results are tabulated in Table 5. It may be observed that P_y and δ_y increase as the amount of reinforcement increases. Also, good agreement between fiber method and conventional calculation results were obtained as indicated by the ratio FM/Calc. This further verifies the accuracy of the fiber method.

For the simulation of the beam with T-EPT system, the following dimensions were used: $X_s=100$ mm, $h_f=200$ mm, and bar diameters for top and bottom bars = 12 mm. This configuration resulted to $P_y=17.0$ kN and $\delta_y=14.685$ mm. After loading and unloading, a residual deflection of 3.334 mm was obtained. Based on fiber method analysis, a jacking force of 100 kN was needed to counteract this residual deflection when $L_{EPT} = 800$ mm. The results of the fiber method

Table 4 Effect of steel frame height, h_f (for $L_{EPT} = 460$ mm)

h_f (mm)	100	150	200	250	300	350	400	450	500
θ (degrees)	18.4	26.6	33.7	39.8	45.0	49.4	53.1	56.3	59.0
L_{EPT}/h_f	4.60	3.07	2.30	1.84	1.53	1.31	1.15	1.02	0.92
P_{ye} (kN)	70	68	66	64	62	62	60	58	58
δ_{ye} (mm)	1.579	1.498	1.446	1.407	1.380	1.481	1.451	1.388	1.451
P_{ye}/P_y	2.33	2.27	2.20	2.13	2.07	2.07	2.00	1.93	1.93
δ_{ye}/δ_y	1.343	1.274	1.230	1.196	1.173	1.259	1.234	1.180	1.234

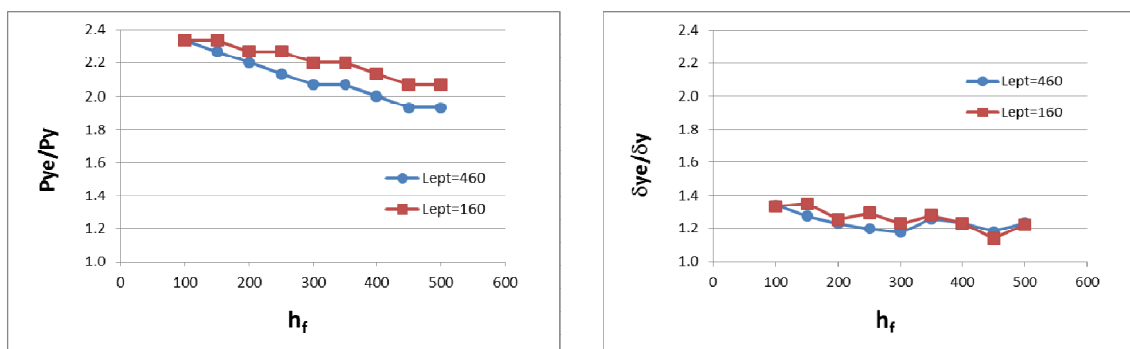
(a) Effect of h_f on load ratios(b) Effect of h_f on deflection ratiosFig. 10 Plot of the effect of h_f on load and deflection ratios

Table 5 Load and deflection at yield of actual-sized beam (200 mm×400 m×6 m)

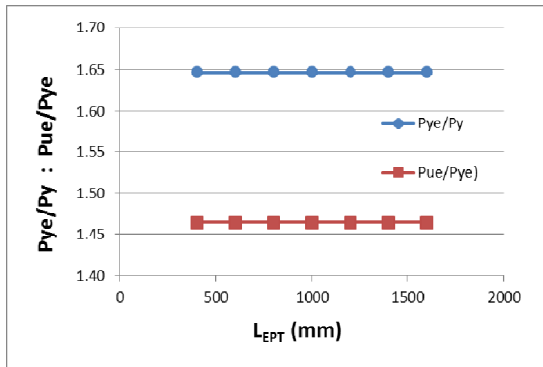
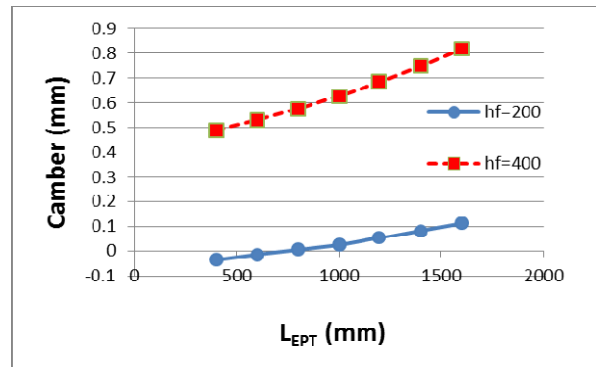
	Bar Dia.	FM	Calc	FM/Calc		Bar Dia.	FM	Calc	FM/Calc
Load at Yield, P_y (kN)	10 mm	13.0	10.7	1.21	Deflection at Yield, δ_y (mm)	10	12.336	12.372	1.00
	12 mm	17.0	15.1	1.13		12	14.685	15.116	0.97
	16 mm	33.0	26.0	1.27		16	20.904	19.228	1.09
	20 mm	48.0	39.3	1.22		20	22.899	21.859	1.05
	25 mm	67.0	59.8	1.12		25	22.911	23.939	0.96

simulations are tabulated in Table 6 for different L_{EPT} . The value of L_{EPT} was varied from 400 mm to 1600 mm. These are the chosen value of L_{EPT} because this is probably the most practical that can be used in actual application. Results indicate that generally the T-EPT increased the strength of the beam. The load at yield, P_{ye} , increased by 65% reckoned from P_y . The load at ultimate, P_{ue} , increased by 46% reckoned from P_{ye} . It can be seen that the value of loads P_{ye} and P_{ue} did not change as L_{EPT} is changed. See also Fig. 11(a). This may be because the L_{EPT}/L is confined only to a narrower range (0.067-0.267). At this range, the smaller beam investigated earlier gave almost constant value.

Another thing that should be noted is the presence of significant camber when L_{EPT} becomes long. In the smaller beams, camber was very small and can be considered zero. Fig. 11(b) shows the resulting camber as affected by the length of the steel frame. Camber is larger for $h_f=400$ mm than that for $h_f=200$ mm. Since the jacking force was the same for all cases, this means that more than the needed jacking force was applied to the beams with longer steel frame resulted to

Table 6 Fiber method results for actual-sized beams as affected by L_{EPT} (for $hf=200$)

L_{EPT} (mm)	400	600	800	1000	1200	1400	1600
L_{EPT}/L	0.067	0.100	0.133	0.167	0.200	0.233	0.267
θ (degrees)	4.2	4.4	4.6	4.8	5.0	5.2	5.4
Pye (kN)	28.0	28.0	28.0	28.0	28.0	28.0	28.0
Pue (kN)	41.0	41.0	41.0	41.0	41.0	41.0	41.0
Pye/Py	1.65	1.65	1.65	1.65	1.65	1.65	1.65
Pue/Pye	1.46	1.46	1.46	1.46	1.46	1.46	1.46
δ_{ye} (mm)	17.513	17.425	17.346	17.290	17.137	17.613	18.134
δ_{ue} (mm)	83.589	82.026	82.060	79.059	80.702	79.053	77.942
δ_{ye}/δ_y	1.19	1.19	1.18	1.18	1.17	1.20	1.23
δ_{ue}/δ_{ye}	4.77	4.71	4.73	4.57	4.71	4.49	4.30
Camber (mm)	-0.036	-0.016	0.005	0.024	0.054	0.082	0.112

(a) Plot of L_{EPT} against load ratios(b) Plot of L_{EPT} against camberFig. 11 Effect of L_{EPT} on the load ratios and camber of actual-sized beam

cambering, especially for $hf=400$ mm.

4.4 Effect of jacking force and initial deflection

One very important thing to consider in T-EPT retrofitting system is the magnitude of the jacking force. Estimating the jacking force by using the deflection formula may not give the correct value unless a realistic correction factor is applied. It is difficult to establish such correction factor similar to that used in Eq. (8) because of the presence of axial force, which tends to close the cracks. Using the fiber method the needed jacking force can be calculated for a given residual displacement. However, to provide a better understanding of the effect of the jacking force, fiber method simulations were done by applying different magnitude of jacking force to the actual-sized beam. For this investigation, the steel frame is chosen to measure as follows: $L_{EPT}=1500$ mm and $hf=200$ mm. The result of the fiber method analysis is tabulated in Table 7.

It can be observed that the loads Pye and Pue increases as the jacking force is increase. This trend is also plotted in Fig. 12(a) and is observed to be linear. Likewise, the deflection at yield, δ_{ye} , increases also as P_j increases (see Table 7). On the other hand, the deflection at ultimate, δ_{ue} ,

Table 7 Fiber method results for actual-sized beam as affected by jacking force, P_j

P_j (kN)	0	25	50	75	100	125	150	175	200
P_{ye} (kN)	16.0	19.0	22.0	26.0	29.0	32.0	35.0	38.0	41.0
P_{ue} (kN)	33.0	35.0	37.0	39.0	41.0	44.0	46.0	49.0	51.0
P_{ye}/P_y	0.94	1.12	1.29	1.53	1.71	1.88	2.06	2.24	2.41
P_{ue}/P_{ye}	2.06	1.84	1.68	1.50	1.41	1.38	1.31	1.29	1.24
δ_{ye} (mm)	17.83	17.70	17.07	18.02	18.11	18.31	18.54	19.02	19.45
δ_{ue} (mm)	154.36	125.33	107.55	93.61	74.83	78.42	66.25	66.68	56.86
δ_{ye}/δ_y	1.21	1.21	1.16	1.23	1.23	1.25	1.26	1.29	1.32
δ_{ue}/δ_{ye}	8.66	7.08	6.30	5.19	4.13	4.28	3.57	3.51	2.92
Camber (mm)	-3.33	-1.74	-0.80	-0.15	0.00	0.26	0.43	0.61	0.80

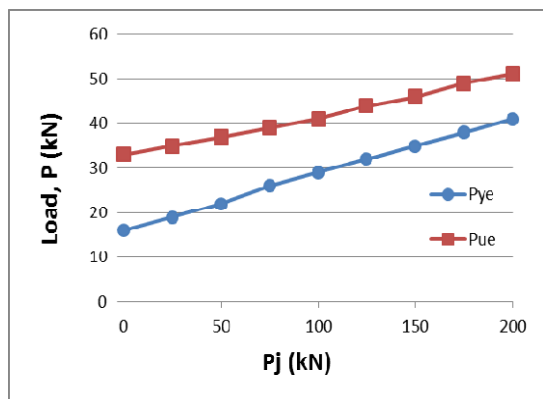
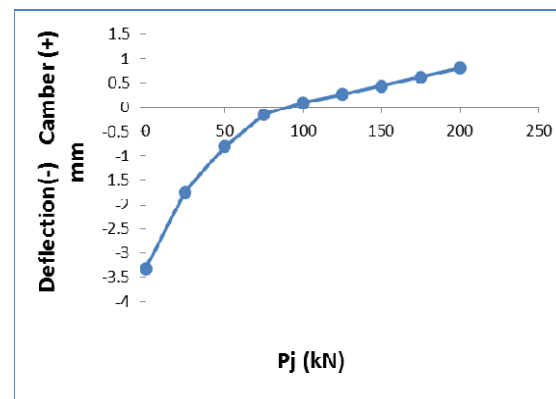
(a) Plot of P_j against load P (b) Plot of P_j against camber

Fig. 12 Effect of jacking force on load carrying capacity and camber

Table 8 Effect of initial deflection

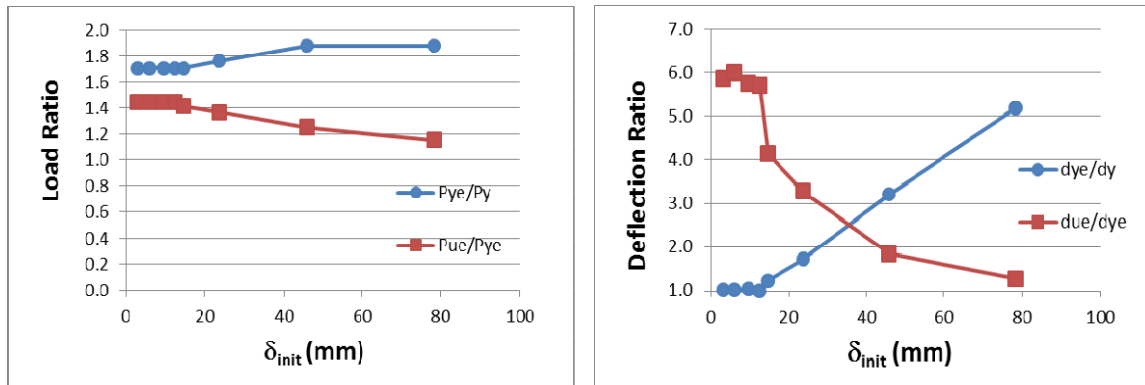
δ_{init} (mm)	3.076	6.020	9.615	12.489	14.685	23.596	45.720	78.253
%	21%	41%	65%	85%	100%	161%	311%	533%
P_{init} (kN)	6.0	10.0	14.0	16.0	17.0	20.0	24.0	28.0
δ_{res} (mm)	0.278	0.438	0.643	0.931	3.334	9.598	35.843	75.562
P_{ye} (kN)	29.0	29.0	29.0	29.0	29.0	30.0	32.0	32.0
P_{ue} (kN)	42.0	42.0	42.0	42.0	41.0	41.0	40.0	37.0
P_{ye}/P_y	1.71	1.71	1.71	1.71	1.71	1.76	1.88	1.88
P_{ue}/P_{ye}	1.45	1.45	1.45	1.45	1.41	1.37	1.25	1.16
δ_{ye} (mm)	14.876	14.837	15.220	14.692	18.106	25.126	47.207	76.116
δ_{ue} (mm)	87.333	89.075	87.574	83.690	74.832	82.433	86.712	96.528
δ_{ye}/δ_y	1.01	1.01	1.04	1.00	1.23	1.71	3.21	5.18
δ_{ue}/δ_{ye}	5.87	6.00	5.75	5.70	4.13	3.28	1.84	1.27
Camber	0.599	0.515	0.406	0.322	0.097	-0.407	-11.541	-40.473

decreases as the P_j increases. This resulted to a decreasing ductility (expressed in terms of δ_{ue}/δ_{ye}) as P_j is increased.

Another obvious behavior that can be observed is the camber. It is produced when the jacking force applied is more than what is required to counteract the residual deflection. In this case, 100kN is the required jacking force. When less than this value is applied, a proportional deflection remained. This behavior is also shown in Fig. 12(b). When the jacking force applied exceeded 100kN, a somewhat linear increase in camber was obtained.

Lastly, the effect of the initial deflection, δ_{init} , is also investigated using the fiber method analysis.

This is done by applying an initial load, P_{init} , to produce the initial deflection. After applying the initial load, it is then unloaded. Then the residual deflection is counter-acted by applying a jacking force, which is maintained at 100kN for all cases. Then the beam is reloaded up to ultimate. The results of the fiber method analysis are tabulated in Table 8.



(a) Plot of δ_{init} against load ratio

(b) Plot of δ_{init} against deflection ratio

Fig. 13 Effect of initial displacement on load ratio and deflection ratio

The initial deflections are also expressed in percentage with respect to δ_y for easy reference. As expected, larger residual deflection is produced when larger initial deflection is applied. The loads P_{ye} and P_{ue} remained the same for initial displacement equal to and less than δ_y ($\delta_{init} \leq \delta_y$). When initial displacement greater than δ_y is applied, P_{ye} increased slightly resulting to the increase in P_{yc}/P_y . On the other hand, P_{ue} decreased. Due to this, the ratio P_{uc}/P_{yc} decreased. This is shown in Fig. 13(a). But overall, the ratios are greater than one, implying that there is an increase in strength in all cases. This means that even if the beam is initially loaded beyond the yield, it can still be effectively strengthened by T-EPT. Also, it is observed that roughly the same increase in strength is obtained as long as the applied jacking force that is needed to counteract a residual displacement resulting from P_y . Also, instead of camber, deflection still remained after the jacking force is applied when the beam is initially loaded beyond the yield. This indicates that higher jacking force is needed when the initial deflection is greater than δ_y .

In Fig. 13(b), the effects of the initial displacement on the deflection ratios are shown. The deflection at yield, δ_{ye} , tends to increase when the initial displacement applied becomes greater than δ_y . This resulted to an almost linearly increasing δ_{yc}/δ_y . However, the ultimate deflection,

δ_{ue} , is almost the same for all values of initial deflection. As a result, the ductility ratio (δ_{ue}/δ_{ye}) decreases as the initial displacement becomes greater than δ_y .

5. Conclusions

The experimental results proved the effectiveness of T-EPT in retrofitting RC beams. To verify this, a fiber method was developed to simulate the behavior of RC beam retrofitted with T-EPT. The results of the fiber method analysis agreed well with the experiment results. It is concluded that the developed fiber method can adequately simulate the behavior of RC beam with T-EPT. The fiber method also provided a means to estimate the required jacking force for the T-EPT system.

Parametric investigation was conducted. It was found out that the dimensions of the braced steel frame affect the effectiveness of the T-EPT. For the small-scaled specimen (used in the experiment), it was observed that the steel frame with shorter length (L_{EPT}) and smaller height (hf) provided higher increase in load carrying capacity of the reinforced beam. In general, better effectiveness is obtained when the slope of the tendon is smaller. This may be used as basis in designing the T-EPT. However, it is recommended to verify the design by doing a fiber method analysis. It was also found out that performance of the beam is affected by the magnitude of the jacking force. The initial deflection has an effect, but the same increase in strength can be obtained as long as adequate jacking force is applied. Findings indicate that ideally the jacking force that should be applied should counteract the residual deflection resulting when the initial displacement of δ_y is applied. In general, the fiber method helped proved that the T-EPT is effective in retrofitting RC beam.

Acknowledgments

The author would like to express gratitude to the University Research Coordinating Office (URCO) of De La Salle University for the opportunity to conduct this research. Acknowledgment is also due to the following: Kenneth Toral, Dustin Grimares, Mikael Peñamante, and Janina Roxas for working hard in doing the experimental tests, and to the faculty and staff of the Civil Engineering Department, De La Salle University for their camaraderie support.

References

- ACI Committee 318 (2008), *Building Code Requirements for Structural Concrete and Commentary*, Farmington Hills, MI.
- Adiaz, P., Vidad, D.J. and Lejano, B. (2011), "Retrofitting of steel wide flange beams using exterior post-tensioning", *Proceedings of the Science and Technology Congress*, Manila, Philippines, February.
- Astillero, C., Barretto, I.G., Brillante, C.C., Provido, W. and Lejano, B. (2013), "Experimental evaluation of the structural performance of deformed wide-flanged beam retrofitted with harped exterior post-tensioning system", *Proceedings of the DLSU Research Congress*, Manila, Philippines, March.
- Au, F.T.K., Chan, K.H.E., Kwan, A.K.H. and Du, J.S. (2009), "Flexural ductility of prestressed concrete beams with unbonded tendons", *Comput. Concrete*, **6**(6), 451-472.

- Bennitz, A., Schmidt, J.W., Nilimaa, J., Taljsten, B., Goltermann, P. and Lund Ravn, D. (2012), "Reinforced concrete t-beams externally prestressed with unbonded carbon fiber-reinforced polymer tendons", *ACI Struct. J.*, **109**(4), 521-530.
- Ciampi, V., Eligenhausen, R., Bertero, V.V. and Popov, E.P. (1982), "Analytical model for concrete anchorages of reinforcing bars under generalized excitation", Report No. UBC/EERC-82/83, Univ. of CA., Berkeley, CA., November.
- Daly, A.F. and Witarnawan, W. (1997), "Strengthening of bridges using external post-tensioning", *Proceedings of the Eastern Asia Society for Transportation Studies (EASTS)*, Seoul, Korea, October.
- Du, J.S., Au, F.T.K., Cheung, Y.K. and Kwan, A.K.H. (2008), "Ductility analysis of prestressed concrete beams with unbonded tendons", *Eng. Struct.*, **30**(1), 13-21.
- El-Shafiey, T. and Atta, A. (2012), "Retrofitting of reinforced concrete beams in shear using external prestressing technique", *Mag. Concrete Res.*, **64**(3), 201-211.
- Elrefai, A., West, J. and Soudki, K. (2012), "Fatigue of reinforced concrete beams strengthened with externally post-tensioned cfrp tendons", *Constr. Build. Mater.*, **29**, 246-256.
- Elrefai, A., West, J. and Soudki, K. (2008), "Effects of overloading on fatigue performance of reinforced concrete beams strengthened with externally post-tensioned carbon-fibre-reinforced polymer tendons", *Can. J. Civ. Eng.*, **35**(11), 1294-1307.
- Kaba, S.A. and Mahin, S.A. (1984), "Refined modeling of reinforced concrete columns for seismic analysis; Report No. UBC/EERC-84/3, Univ. of California, Berkeley, CA, April.
- Kim, K.S. and Lee, D.H. (2012), "Flexural behavior model for post-tensioned concrete members with unbonded tendons", *Comput. Concrete*, **10**(3), 241-257.
- Kitajima, K. (1994), "Study on response characteristics of reinforced concrete building under bidirectional earthquake motions", Doctoral Dissertation, Nihon University, Japan. (in Japanese)
- Klaiber, F.W., Dunken, K.F. and Sanders, W.W.Jr (1981), "Feasibility study of strengthening existing single span steel beam concrete deck bridges", *Eng. Res.*, June.
- Lee, D.H. and Kim, K.S. (2011), "Flexural strength of prestressed concrete members with unbonded tendons", *Struct. Eng. Mech.*, **38**(5), 675-696.
- Lee, S.H., Shin, K.J. and Kang, T.H.K. (2015), "Flexural strengthening of continuous concrete beams using external prestressed steel bars", *PCI J.*, **60**(1), 68-86.
- Lee, S.H., Yeo, U.S., Shin, K.J. and Kim, W.J. (2010), "Analytical study on strengthening effect of RC beams strengthened with high-tension steel rod", *Struct. Congress*, 3590-3601.
- Lejano, B.A. (1995), "Study on the flexural and shear behavior of high strength reinforced concrete columns subjected to high and fluctuating axial load", Doctoral Dissertation, Nihon University, Chiba, Japan.
- Lejano, B. (2007), "Investigation of biaxial bending of reinforced concrete columns through fiber method modeling", *J. Res. Sci. Comput. Eng.*, **4**(3), 61-73.
- Lejano, B. (2009), "Modeling the stress-strain relationship of high strength concrete made of local aggregates", *Proceedings of the 1st ASEAN Civil Engineering Conference (ACEC)*, Pattaya, Thailand, AUN-Seed Net, March.
- Lou, T. and Xiang, Y. (2006), "Finite element modeling of concrete beams prestressed with external tendons", *Eng. Struct.*, **28**(14), 1919-1926.
- Lou, T., Lopes, S.M.R. and Lopes, A.V. (2013), "Flexural response of continuous concrete beams prestressed with external tendons", *J. Bridge Eng.*, **18**(6), 525-537.
- Mark, K.M.S. and Roesset, J.M. (1976), "Nonlinear dynamic response of reinforced concrete frames," Publication R76-38, Department of Civil Engineering, M.I.T., August.
- Matta, F., Nanni, A., Abdelrazaq, A., Gremel, D. and Koch, R. (2009), "Externally post-tensioned carbon frp bar system for deflection control", *Constr. Build. Mater.*, **23**(4), 1628-1639.
- Mullapudi, T.R.S. and Ayoub, A.S. (2013), "Analysis of reinforced concrete columns subjected to combined axial, flexure, shear and torsional loads", *J. Struct. Eng.*, **139**(4), 561-573.
- Naghypour, M., Nemati, M. and Doostdar, H.M. (2010), "Experimental study and modeling of reinforced concrete beams strengthened by post-tensioned external reinforcing bars", *IJE Tran. A: Basic.*, **23**(2), 127-144.

- Nordin, H. (2005), "Strengthening structures with externally prestressed tendons-literature review", Technical Report, Department of Civil and Environmental Engineering, Division of Structural Engineering, Luleå University of Technology, December.
- Park, R. and Paulay, T. (1975), *Reinforced Concrete Structures*, 1st Edition, John Wiley & Sons, Inc., New York, USA.
- Peñamante, M., Grimares, D., Roxas, J.R., Toral, K.R. and Lejano, B. (2015), "Structural retrofitting of reinforced concrete beams using turnbuckle exterior post-tensioning", *Proceedings of the DLSU Research Congress*, Manila, Philippines, March.
- Shin, K.J., Lee, S.H. and Kang, T.H.K. (2014), "External posttensioning of reinforced concrete beams using a v-shaped steel rod system", *J. Struct. Eng.*, **140**(3), 04013067.
- Shin, K.J. and Lee, S.H. (2010), "Flexural behaviour of rc beams strengthened with high-tension steel bar", *Mag. Concrete Res.*, **62**(2), 137-147.
- Spacone, E., Filippou, F.C. and Taucer, F.F. (1996), "Fibre beam-column model for nonlinear analysis of r/c frames, part I formulation", *Earthq. Eng. Struct. Dy.*, **25**(7), 711-725.
- Shirai, N., Lejano, B.A., Adachi, H. and Nakanishi, M. (1996), "Flexure and shear behavior of high strength reinforced concrete column subjected to high and fluctuating axial load", *Proceedings of the 11th World Conference on Earthquake Engineering*, Paper No. 1199, Acapulco, Mexico, June.
- Suprenant, B.A. and Malisch, W.R. (2009), *Effect of Post-Tensioning on Tolerances*, Concrete International Magazine, January.
- Tan, K.H. and Kong, D.C. (2009), "A direct design approach for strengthening simple-span beams with external posttensioning", *PCI J.*, **54**(4), 48-72.
- Toral, K.R. and Lejano, B.A. (2015), "Analyzing the effectiveness of the turnbuckle exterior post-tensioning as a structural retrofitting method using SAP2000", *Proceedings of the DLSU Research Congress*, Manila, Philippines, March.